

# LETTER

## A massive, quiescent, population II galaxy at a redshift of 2.1

Mariska Kriek<sup>1</sup>, Charlie Conroy<sup>2</sup>, Pieter G. van Dokkum<sup>3</sup>, Alice E. Shapley<sup>4</sup>, Jieun Choi<sup>2</sup>, Naveen A. Reddy<sup>5</sup>, Brian Siana<sup>5</sup>, Freeke van de Voort<sup>1</sup>, Alison L. Coil<sup>6</sup>, Bahram Mobasher<sup>5</sup>

Unlike spiral galaxies such as the Milky Way, the majority of the stars in massive elliptical galaxies were formed in a short period early in the history of the Universe. The duration of this formation period can be measured using the ratio of magnesium to iron abundance ( $[\text{Mg}/\text{Fe}]$ )<sup>1-4</sup>, which reflects the relative enrichment by core-collapse and type Ia supernovae. For local galaxies,  $[\text{Mg}/\text{Fe}]$  probes the combined formation history of all stars currently in the galaxy, including younger and metal-poor stars that were added during late-time mergers<sup>5</sup>. Therefore, to directly constrain the initial star-formation period, we must study galaxies at earlier epochs. The most distant galaxy for which  $[\text{Mg}/\text{Fe}]$  had previously been measured<sup>6</sup> is at a redshift of  $z \approx 1.4$ , with  $[\text{Mg}/\text{Fe}] = 0.45^{+0.05}_{-0.19}$ . A slightly earlier epoch ( $z \approx 1.6$ ) was probed by stacking the spectra of 24 massive quiescent galaxies, yielding an average  $[\text{Mg}/\text{Fe}]$  of  $0.31 \pm 0.12$ <sup>7</sup>. However, the relatively low signal-to-noise ratio of the data and the use of index analysis techniques for both studies resulted in measurement errors that are too large to allow us to form strong conclusions. Deeper spectra at even earlier epochs in combination with analysis techniques based on full spectral fitting are required to precisely measure the abundance pattern shortly after the major star-forming phase ( $z > 2$ ). Here we report a measurement of  $[\text{Mg}/\text{Fe}]$  for a massive quiescent galaxy at a redshift of  $z = 2.1$ , when the Universe was 3 billion years old. With  $[\text{Mg}/\text{Fe}] = 0.59 \pm 0.11$ , this galaxy is the most Mg-enhanced massive galaxy found so far, having twice the Mg enhancement of similar-mass galaxies today. The abundance pattern of the galaxy is consistent with enrichment exclusively by core-collapse supernovae and with a star-formation timescale of 0.1 to 0.5 billion years – characteristics that are similar to population II stars in the Milky Way. With an average past star-formation rate of 600 to 3,000 solar masses per year, this galaxy was among the most vigorous star-forming galaxies in the Universe.

We observed the galaxy COSMOS-11494 with the near-infrared multi-object spectrograph MOSFIRE on the *Keck I Telescope*<sup>8</sup>. It was also observed by two other programmes<sup>9,10</sup>, and so we incorporated these publicly available archival data. COSMOS-11494 was selected from the 3D-HST survey<sup>11,12</sup>. With a stellar mass  $M$  given by  $\log_{10} M/M_{\odot} = 11.5 \pm 0.1$ , COSMOS-11494 is among the most massive galaxies at its redshift, and it has a very low star-formation rate of less than  $0.6 M_{\odot}/\text{yr}$  (see Methods). Similarly to the typical massive, quiescent galaxy at this redshift, it is smaller than its local counterparts of the same mass, with an effective radius of 2.1 kpc<sup>13</sup>. The MOS-

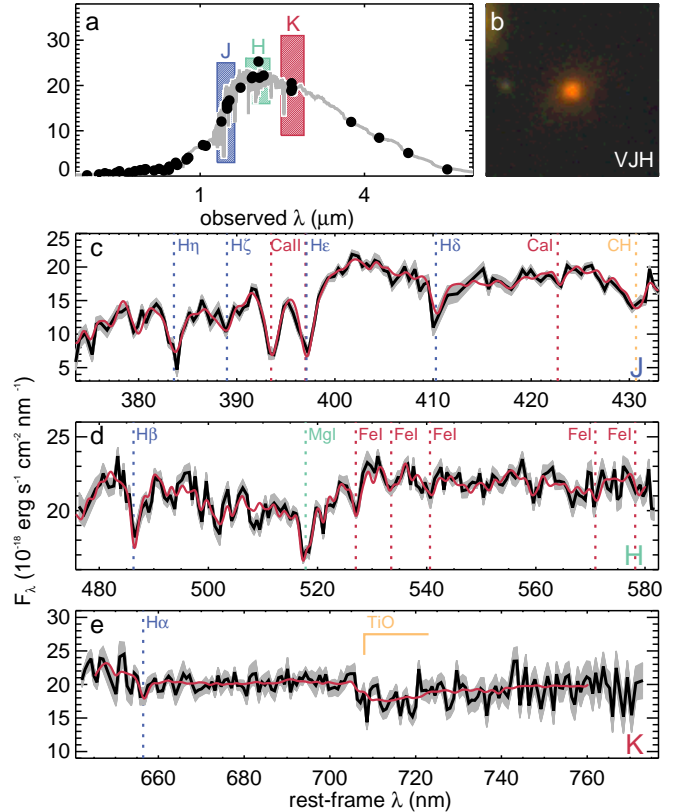


Figure 1: **Photometry, image and MOSFIRE spectrum of COSMOS-11494.** **a**, Multi-wavelength spectral energy distribution (black circles) and best-fitting stellar population model to only the photometry (grey line). **b**, *HST* colour (V, J, and H) image. **c-e**, MOSFIRE spectrum in three wavelength intervals (J, H, and K; black), corresponding to the coloured areas in **a**. The gray shaded regions represent the  $1\sigma$  uncertainty on the flux. The best-fitting stellar population model used to derive the age and abundance pattern is shown in red.

FIRE rest-frame optical spectrum, the multi-wavelength spectral energy distribution<sup>11</sup> and *Hubble Space Telescope* (*HST*) colour image<sup>11</sup> of COSMOS-11494 are shown in Figure 1.

Here we measure the stellar abundance pattern of COSMOS-11494 from the MOSFIRE rest-frame optical spectrum with our absorption line fitter (`a1f`) code<sup>14</sup> (see Methods). For our default model we adopt a two-component stellar population, for which the age of both components and the slope of the stellar initial mass function (IMF) are free parameters. To enable comparison with previous work<sup>15</sup>, we also fit

<sup>1</sup>Department of Astronomy, University of California, Berkeley, CA 94720, USA <sup>2</sup>Department of Astronomy, Harvard University, Cambridge, MA, USA <sup>3</sup>Astronomy Department, Yale University, New Haven, CT, USA <sup>4</sup>Department of Physics & Astronomy, University of California, Los Angeles, CA 90095, USA <sup>5</sup>Department of Physics & Astronomy, University of California, Riverside, CA 92521, USA <sup>6</sup>Center for Astrophysics and Space Sciences, University of California, San Diego, La Jolla, CA 92093, USA

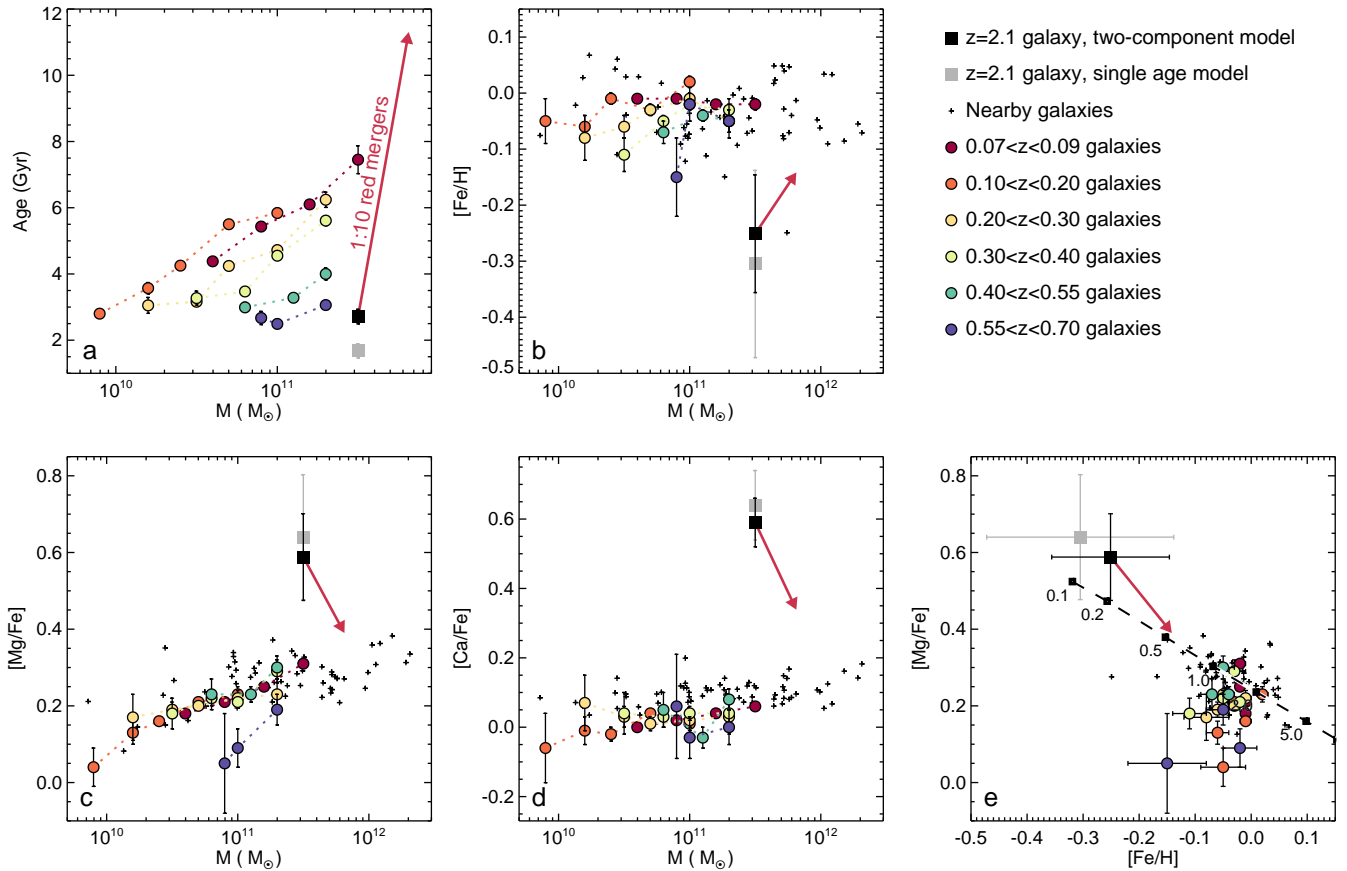


Figure 2: **Age and abundance patterns of COSMOS-11494 in comparison to lower-redshift quiescent galaxies.** **a**, Stellar population age, **b**,  $[\text{Fe}/\text{H}]$ , **c**,  $[\text{Mg}/\text{Fe}]$ , and **d**,  $[\text{Ca}/\text{Fe}]$  versus stellar mass. **e**,  $[\text{Mg}/\text{Fe}]$  versus  $[\text{Fe}/\text{H}]$ . The black dashed line represents a chemical evolution model for different star-formation timescales in Gyr. In all panels, the black and grey filled squares represent COSMOS-11494 for the two-component and single-age model, respectively, the coloured symbols represent low-redshift galaxies<sup>15</sup> binned by mass and redshift, and the small black pluses are nearby galaxies<sup>17</sup>. Error bars are  $1\sigma$ . The red arrows represent the simple evolutionary model (see main text).

the spectrum with a single-age model and a Kroupa<sup>16</sup> IMF.

For the default model we find  $[\text{Fe}/\text{H}] = -0.25 \pm 0.11$ ,  $[\text{Mg}/\text{Fe}] = 0.59 \pm 0.11$ ,  $[\text{Ca}/\text{Fe}] = 0.59 \pm 0.07$  and an age of  $2.71 \pm 0.22$  Gyr. The best-fitting mass-to-light ratio ( $M/L$ ) is consistent with the  $M/L$  assuming a Kroupa IMF ( $(M/L)/(M/L_{\text{Kroupa}}) = 0.97 \pm 0.55$ ), although the error is large because of the insufficient S/N of the spectrum and the lack of rest-frame near-infrared coverage. We also fit this model with  $\lambda_{\text{restframe}} < 4000 \text{ \AA}$  excluded, and find similar values. For the single-age model we find similar abundance ratios as for the two-component model, but the modelled age is 1 Gyr younger. This difference is expected, because younger stellar populations have lower  $M/L$  and so have larger weights in the fit.

In Figure 2 we compare the spectral modelling results of COSMOS-11494 with those of galaxies at  $0.05 < z < 0.7$ <sup>15</sup> and of a sample of nearby massive galaxies<sup>17</sup>. All galaxies are fitted with the `alf` code. Figure 2 illustrates that COSMOS-11494 is more Mg-enhanced than similar-mass galaxies at lower redshift, with  $[\text{Mg}/\text{Fe}]$  about 0.3 dex higher.  $[\text{Ca}/\text{Fe}]$  is also higher compared to the values for lower-redshift massive galaxies.

To interpret the abundance pattern of COSMOS-11494, we show a chemical evolution model in Figure 2e, which assumes a Salpeter IMF<sup>18</sup>, a constant star-formation history over a given timescale, a core-collapse<sup>19</sup> and a type Ia supernova yield model<sup>20</sup>; we also adopt a power-law delay-time distribution of the form  $t^{-1}$  for type Ia supernovae that occurred between 0.1 and 13 Gyr<sup>21</sup>. The star-formation

timescale decreases along the curve, with the highest value of  $[\text{Mg}/\text{Fe}]$  corresponding to the shortest timescale of 0.1 Gyr. The relatively low Fe abundance in combination with the high  $[\text{Mg}/\text{Fe}]$  favours a short star-formation timescale of around 0.2 Gyr. Therefore, this model implies that COSMOS-11494 has experienced very little enrichment by type Ia supernovae.

However, the best-fitting timescale strongly depends on the assumed delay time of prompt type Ia supernovae. This parameter is poorly constrained in models and depends on the type Ia progenitor model<sup>22</sup>; for the double degenerate scenario the lifetime can be as short as about 0.1 Gyr, whereas for a single degenerate scenario it can be as high as about 0.5 Gyr<sup>22</sup>. However, the delay times of prompt type Ia supernovae inferred from observations are as short as 0.1 Gyr<sup>21</sup>, and so 0.5 Gyr may be a conservative upper limit. The assumed IMF affects the chemical evolution model as well, and a flatter IMF results in a longer timescale. Finally, the adopted chemical evolution model depends on the core-collapse supernova yields<sup>19</sup>, and other yield models were unable to reproduce the observed high  $[\text{Mg}/\text{Fe}]$  in combination with the observed  $[\text{Fe}/\text{H}]$ <sup>23,24</sup>. Nonetheless, individual stars with similarly high  $[\text{Mg}/\text{Fe}]$  and  $[\text{Fe}/\text{H}]$  values as COSMOS-11494 have been identified in the bulge of the Milky Way<sup>25</sup>, which supports the validity of the adopted yield model<sup>19</sup>. Taking into account all uncertainties on our chemical evolution model, we estimate a star-formation timescale of  $\sim 0.1 - 0.5$  Gyr.

Ca, which is also produced and returned to the interstellar medium

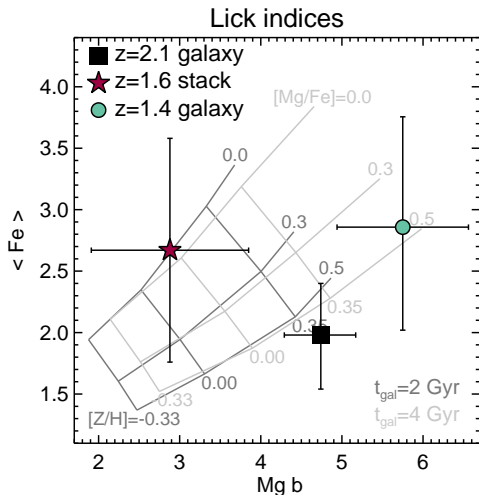


Figure 3: **Abundance pattern of COSMOS-11494 in comparison to other high-redshifts galaxies.** We show the Lick indices  $\langle \text{Fe} \rangle$  and  $\text{Mg } b$  for COSMOS-11494, a  $z \approx 1.4$  quiescent galaxy<sup>6</sup> observed with *VLT/X-Shooter*, and a stack of  $z \approx 1.6$  quiescent galaxy spectra<sup>7</sup> observed with *Subaru/MOIRCS*. Error bars are  $1\sigma$ . We also show grids based on SPS models<sup>28</sup> for a range of range of values of  $[\text{Z}/\text{H}]$  and  $[\text{Mg}/\text{Fe}]$ . The dark and light grey grids are for galaxy ages of 2 Gyr and 4 Gyr, respectively.

through core-collapse supernovae, also shows a strong enhancement with respect to Fe; the difference compared to low-redshift analogues is even more extreme than for Mg. This differential evolution of Ca and Mg with time is unexpected, because both elements are formed in massive stars, but metallicity-dependent core-collapse-supernova yields might explain the differences<sup>19</sup>.

When combining the star-formation timescale and the best-fitting stellar mass, we find an average past star-formation rate of (600–3,000)  $M_{\odot}/\text{yr}$ . The single-age best-fitting SPS model sets a lower limit on the formation redshift of  $z > 4$ . For the two-component model we find an average formation redshift of  $z = 12_{-4}^{+9}$ . The inferred star-formation rate and formation epoch are consistent with the properties that were derived for the most active galaxy found so far, HFLS3<sup>26</sup>. This dusty sub-millimetre galaxy has a star-formation rate of 2,900  $M_{\odot}/\text{yr}$  and a redshift of  $z = 6.34$ , and so could be similar to the star-forming progenitor of COSMOS-11494.

COSMOS-11494 seems to be more Mg-enhanced than  $z \approx 1.5$  galaxies in previous work. However, because different methods have been used in these studies, systematic differences may occur, and the derived values cannot be directly compared<sup>4</sup>. For a more direct comparison to previous studies, we use the Lick indices<sup>27</sup>  $\langle \text{Fe} \rangle$  ( $=[\text{Fe}5270+\text{Fe}5335]/2$ ) and  $\text{Mg } b$ . For the  $z = 1.4$  galaxy, the spectrum was not deep enough to measure the two Fe lines needed to determine  $\langle \text{Fe} \rangle$ . Instead, we calibrated  $\langle \text{Fe} \rangle$  for two other iron lines (Fe4388 and Fe5015) using a set of SPS models<sup>28</sup>, and derived  $\langle \text{Fe} \rangle$  from these (marginally detected) lines for the  $z = 1.4$  galaxy. Figure 3 shows the measurements in comparison to a grid of SPS models<sup>28</sup> for a range of metallicities ( $[\text{Z}/\text{H}] = -0.33, 0.0, 0.35$ ) and  $[\text{Mg}/\text{Fe}]$  values (0.0, 0.3, 0.5).

For COSMOS-11494 the  $[\text{Mg}/\text{Fe}] \approx 0.6$  implied from the Lick indices is consistent with the modelling results. This value illustrates that COSMOS-11494 – which probes an earlier epoch than previous work – is indeed more Mg-enhanced than the quiescent galaxies in the other studies. Furthermore, our high S/N spectrum results in the most robust abundance pattern measurement for a distant galaxy so far. Although the two different approaches to derive the abundance pattern

give consistent results for COSMOS-11494, for distant galaxies, the full spectral modelling approach is strongly preferred over the approach involving Lick indices (Methods).

The high  $[\text{Mg}/\text{Fe}]$  of COSMOS-11494 compared to lower-redshift quiescent galaxies of similar mass suggests that this galaxy, and possibly other distant quiescent galaxies, do not passively evolve into quiescent early-type galaxies today. A similar conclusion was drawn from the small sizes of distant quiescent galaxies compared to their local analogs<sup>29</sup>, and in the past several years it has become apparent that distant quiescent galaxies grow in mass and size by accreting primarily smaller galaxies<sup>5,30</sup>. This inside-out growth by late-time mergers with less-massive galaxies predicts a decline in  $[\text{Mg}/\text{Fe}]$ , because lower-mass galaxies are less Mg-enhanced<sup>3,15</sup>.

In Figure 2 we explore this scenario by showing the predicted path of COSMOS-11494 for a simple evolutionary model. We assume that the galaxy grows by red minor (1:10) mergers with smaller, less Mg-enhanced quiescent galaxies with  $[\text{Mg}/\text{Fe}] = 0.18$ ,  $[\text{Fe}/\text{H}] = -0.05$ , and  $[\text{Ca}/\text{Fe}] = 0.02$ <sup>15</sup>, and that the mass nearly doubles between  $z = 2.1$  and the present day<sup>5</sup> following the mass evolution  $d(\log M)/dz = -0.15$ . Therefore, we assume no evolution in  $[\text{Mg}/\text{Fe}]$  and  $[\text{Ca}/\text{Fe}]$  at lower masses. If the abundance ratios for these galaxies would be higher at earlier times as well, then the predicted evolution would be less strong. To estimate the evolution in galaxy age for the merger model, we assume that the age is proportional to  $M^{0.3}$ , as was found for  $z < 0.7$  galaxies<sup>15</sup>.

Figure 2 shows that the merger model can substantially decrease  $[\text{Mg}/\text{Fe}]$  and  $[\text{Ca}/\text{Fe}]$ , and increase  $[\text{Fe}/\text{H}]$ . However, there are several caveats to our simple model comparison. First, the  $0.07 < z < 0.7$  measurements are derived by fitting a single-age model, and so are sensitive to low levels of recent star formation. Second, we assume that the accreted stars are well-mixed with the *in-situ* population. However, simulations of galaxy formation show that the added material is mostly deposited in the outskirts of the galaxy<sup>30</sup>, and so the net evolution due to mergers – in the central parts targeted by the spectrographs – may be less. Third, it is unlikely that the descendant of COSMOS-11494 is a typical massive, quiescent galaxy today. The star formation in many low-redshift quiescent galaxies is quenched at later times, resulting in longer star-forming periods and, hence, lower  $[\text{Mg}/\text{Fe}]$ . Therefore, the descendant of COSMOS-11494 presumably resides in the tail of the low-redshift distributions. Finally, the model does not include possible late-time star formation or mergers with star-forming galaxies, which would also result in a decrease in  $[\text{Mg}/\text{Fe}]$  with time.

More spectra of quiescent galaxies at high redshifts are needed to measure the evolution of the slope and the intercept of the age –  $M$  and  $[\text{Mg}/\text{Fe}] - M$  relation. These measurements could eventually discriminate between different evolutionary scenarios, and the amount of mixing of stars after galaxy mergers<sup>15</sup>. In combination with more accurate supernova progenitor and yield models, and therefore improved chemical evolution models, these measurements will also provide unique information on the star-formation histories of the most massive galaxies and their possible role in the reionization of the Universe at  $z > 6$ . We expect that observations with NIRSpec on the *James Webb Space Telescope* will revolutionize this field within the next five years, with future ultra-deep observations with MOSFIRE paving the way.

1. Matteucci, F. Abundance ratios in ellipticals and galaxy formation. *Astron. Astrophys.* **288**, 57–64 (1994).
2. Trager, S. C., Faber, S. M., Worthey, G. & González, J. J. The Stellar Population Histories of Early-Type Galaxies. II. Controlling Parameters of the Stellar Populations. *Astron. J.* **120**, 165–188 (2000).
3. Thomas, D., Maraston, C., Bender, R. & Mendes de Oliveira, C. The Epochs of Early-Type Galaxy Formation as a Function of Environment. *Astrophys. J.* **621**, 673–694 (2005).

4. Conroy, C., Graves, G. J. & van Dokkum, P. G. Early-type Galaxy Archeology: Ages, Abundance Ratios, and Effective Temperatures from Full-spectrum Fitting. *Astrophys. J.* **780**, 33 (2014).
5. van Dokkum, P. G. *et al.* The Growth of Massive Galaxies Since  $z = 2$ . *Astrophys. J.* **709**, 1018–1041 (2010).
6. Lonoce, I. *et al.* Old age and supersolar metallicity in a massive  $z \sim 1.4$  early-type galaxy from VLT/X-Shooter spectroscopy. *Mon. Not. R. Astron. Soc.* **454**, 3912–3919 (2015).
7. Onodera, M. *et al.* The Ages, Metallicities, and Element Abundance Ratios of Massive Quenched Galaxies at  $z \simeq 1.6$ . *Astrophys. J.* **808**, 161 (2015).
8. McLean, I. S. *et al.* MOSFIRE, the multi-object spectrometer for infrared exploration at the Keck Observatory. In *Society of Photo-Optical Instrumentation Engineers (SPIE) Conference Series*, vol. 8446 of *Society of Photo-Optical Instrumentation Engineers (SPIE) Conference Series* (2012).
9. Belli, S., Newman, A. B., Ellis, R. S. & Konidaris, N. P. MOSFIRE Absorption Line Spectroscopy of  $z > 2$  Quiescent Galaxies: Probing a Period of Rapid Size Growth. *Astrophys. J. Let.* **788**, L29 (2014).
10. Kriek, M. *et al.* The MOSFIRE Deep Evolution Field (MOSDEF) Survey: Rest-frame Optical Spectroscopy for  $\sim 1500$  H-selected Galaxies at  $1.37 \leq z \leq 3.8$ . *Astrophys. J. Supp.* **218**, 15 (2015).
11. Skelton, R. E. *et al.* 3D-HST WFC3-selected Photometric Catalogs in the Five CANDELS/3D-HST Fields: Photometry, Photometric Redshifts, and Stellar Masses. *Astrophys. J. Supp.* **214**, 24 (2014).
12. Momcheva, I. G. *et al.* The 3D-HST Survey: Hubble Space Telescope WFC3/G141 grism spectra, redshifts, and emission line measurements for  $\sim 100,000$  galaxies. *ArXiv e-prints* (2015).
13. van de Sande, J. *et al.* Stellar Kinematics of  $z \sim 2$  Galaxies and the Inside-out Growth of Quiescent Galaxies. *Astrophys. J.* **771**, 85 (2013).
14. Conroy, C. & van Dokkum, P. Counting Low-mass Stars in Integrated Light. *Astrophys. J.* **747**, 69 (2012).
15. Choi, J. *et al.* The Assembly Histories of Quiescent Galaxies since  $z = 0.7$  from Absorption Line Spectroscopy. *Astrophys. J.* **792**, 95 (2014).
16. Kroupa, P. On the variation of the initial mass function. *Mon. Not. R. Astron. Soc.* **322**, 231–246 (2001).
17. Conroy, C. & van Dokkum, P. G. The Stellar Initial Mass Function in Early-type Galaxies From Absorption Line Spectroscopy. II. Results. *Astrophys. J.* **760**, 71 (2012).
18. Salpeter, E. E. The Luminosity Function and Stellar Evolution. *Astrophys. J.* **121**, 161 (1955).
19. Kobayashi, C., Umeda, H., Nomoto, K., Tominaga, N. & Ohkubo, T. Galactic Chemical Evolution: Carbon through Zinc. *Astrophys. J.* **653**, 1145–1171 (2006).
20. Nomoto, K., Thielemann, F.-K. & Yokoi, K. Accreting white dwarf models of Type I supernovae. III - Carbon deflagration supernovae. *Astrophys. J.* **286**, 644–658 (1984).
21. Maoz, D., Mannucci, F. & Brandt, T. D. The delay-time distribution of Type Ia supernovae from Sloan II. *Mon. Not. R. Astron. Soc.* **426**, 3282–3294 (2012).
22. Kobayashi, C. & Nomoto, K. The Role of Type Ia Supernovae in Chemical Evolution. I. Lifetime of Type Ia Supernovae and Metallicity Effect. *Astrophys. J.* **707**, 1466–1484 (2009).
23. Thielemann, F.-K., Nomoto, K. & Hashimoto, M.-A. Core-Collapse Supernovae and Their Ejecta. *Astrophys. J.* **460**, 408 (1996).
24. Woosley, S. E. & Weaver, T. A. The Evolution and Explosion of Massive Stars. II. Explosive Hydrodynamics and Nucleosynthesis. *Astrophys. J. Supp.* **101**, 181 (1995).
25. Fulbright, J. P., McWilliam, A. & Rich, R. M. Abundances of Baade's Window Giants from Keck HIRES Spectra. II. The Alpha and Light Odd Elements. *Astrophys. J.* **661**, 1152–1179 (2007).
26. Riechers, D. A. *et al.* A dust-obscured massive maximum-starburst galaxy at a redshift of 6.34. *Nature* **496**, 329–333 (2013).
27. Worthey, G., Faber, S. M., Gonzalez, J. J. & Burstein, D. Old stellar populations. 5: Absorption feature indices for the complete LICK/IDS sample of stars. *Astrophys. J. Supp.* **94**, 687–722 (1994).
28. Thomas, D., Maraston, C. & Bender, R. Stellar population models of Lick indices with variable element abundance ratios. *Mon. Not. R. Astron. Soc.* **339**, 897–911 (2003).
29. van Dokkum, P. G. *et al.* Confirmation of the Remarkable Compactness of Massive Quiescent Galaxies at  $z \sim 2.3$ : Early-Type Galaxies Did not Form in a Simple Monolithic Collapse. *Astrophys. J. Let.* **677**, L5–L8 (2008).
30. Naab, T., Johansson, P. H. & Ostriker, J. P. Minor Mergers and the Size Evolution of Elliptical Galaxies. *Astrophys. J. Let.* **699**, L178–L182 (2009).

**Acknowledgements** M. K. acknowledges discussions with J. Greene and E. Quataert. The data presented in this paper were obtained at the W.M. Keck Observatory, which is operated as a scientific partnership among the California Institute of Technology, the University of California and the National Aeronautics and Space Administration. The Observatory was made possible by the generous financial support of the W.M. Keck Foundation. The authors wish to recognize and acknowledge the very significant cultural role and reverence that the summit of Mauna Kea has always had within the indigenous Hawaiian community. We are most fortunate to have the opportunity to conduct observations from this mountain. We acknowledge support from NSF AAG collaborative grants AST-1312780, 1312547, 1312764, and 1313171 and archival grant AR-13907, provided by NASA through a grant from the Space Telescope Science Institute. C.C. acknowledges support from NASA grant NNX13AI46G, NSF grant AST-1313280, and the Packard Foundation.

**Correspondence** Correspondence and requests for materials should be addressed to M. K. (email: mkriek@berkeley.edu).

**Author Contributions** M. K., P. G. v. D. & C. C., wrote the primary Keck proposal. M. K. & C. C. led the interpretation. M. K. wrote the reduction pipeline, reduced the data, determined the stellar mass, measured the Lick indices, and wrote the text. C. C. developed the SPS model, fitted the spectrum, and derived the chemical evolution model. M. K., P. G. v. D., J. C., F. v. d. V., and N. A. R. did the observations. All authors contributed to the analysis and interpretation.

## METHODS

**Best-fitting model to the photometry.** To derive the stellar mass of COSMOS-11494, we fit the broadband photometry with the flexible stellar population synthesis (SPS) models<sup>31,32</sup>. We assume a delayed exponential star formation history of the form  $\text{SFR} \propto t e^{-t/\tau}$  and the dust attenuation law from Kriek & Conroy<sup>33</sup>. We adopt the Chabrier stellar IMF<sup>34</sup> to facilitate direct comparison with lower-redshift studies<sup>15</sup>.

The error bar on the stellar mass is completely dominated by systematic uncertainties. We estimate this uncertainty by varying the SPS model<sup>35,36</sup>, dust attenuation law<sup>37,38</sup>, parameterization of the star formation history, and the scaling of the broadband spectral energy distribution. We do not vary the IMF, as it can be approximated by a simple offset in the stellar mass. A Kroupa IMF<sup>16</sup> would have resulted in a similar stellar mass as for the Chabrier IMF, whereas a Salpeter IMF<sup>18</sup> would have resulted in a stellar mass a factor of 1.6 higher.

**Spectral fitting.** Parameters are estimated from the rest-frame optical spectrum with the `alf`<sup>4,14,15</sup> code. This code combines libraries of isochrones and empirical stellar spectra with synthetic stellar spectra covering a wide range of elemental abundance patterns. The code fits for C, N, O, Na, Mg, Ca, Ti, V, Cr, Mn, Fe, Co, Ni, redshift, velocity dispersion, and several emission lines. The stellar population age and IMF are free parameters as well, and multiple stellar population components are allowed. When fitting a two-component model, the age represents the mass-weighted average age of the two separate components. The ratio of the model and data are fitted by a high order polynomial to avoid potential issues with the flux calibration of the data. The fitting is done using a Markov chain Monte Carlo algorithm<sup>39</sup>.

**Lick indices versus full spectral modelling.** As mentioned in the main text, for COSMOS-11494 the  $[\text{Mg}/\text{Fe}] \approx 0.6$  implied from the Lick indices is consistent with the modelling results. The metallicity measurements also agree between the two methods: our best-fitting values for  $[\text{Mg}/\text{Fe}]$  and  $[\text{Fe}/\text{H}]$  imply  $[\text{Z}/\text{H}] = 0.25$  ( $=[\text{Fe}/\text{H}] + 0.94[\text{Mg}/\text{Fe}]^{28}$ ), which is consistent with the model shown in Figure 3 for the best-fitting age of 2.5 Gyr. For the  $z \approx 1.4$  individual galaxy and the  $z \sim 1.6$  stack, the abundance patterns are based on the Lick indices, and so by construction they should be closer to the grid points. This is indeed the case for  $z \approx 1.4$  individual galaxy<sup>6</sup> with a  $[\text{Mg}/\text{Fe}]$  of  $0.45_{-0.19}^{+0.05}$  and a  $[\text{Z}/\text{H}]$  of  $0.61_{-0.05}^{+0.06}$ . For the derived age of 4 Gyr the two Lick indices are consistent with the model grid. However, the individual Fe lines yield very different and inconsistent results when calculating  $\langle \text{Fe} \rangle$ . For the  $z \approx 1.6$  galaxy stack<sup>7</sup>, the derived  $[\text{Mg}/\text{Fe}] = 0.31_{-0.12}^{+0.12}$ ,  $[\text{Z}/\text{H}] = 0.24_{-0.14}^{+0.20}$  and  $\log(\text{age}/\text{Gyr}) = 0.04_{-0.08}^{+0.10}$  are less consistent with the derived values based on all Lick indices, though the error bars are large.

Although the two different approaches to derive the abundance pattern agree well for COSMOS-11494, the full spectral modelling approach is strongly preferred over the approach involving Lick indices. The rest-frame optical spectrum of  $z > 1$  galaxies has been shifted to near-infrared wavelengths. The many skylines at these wavelengths in combination with the relatively lower S/N of the spectra of distant galaxies result in large error bars on the measurement of a single feature. Lick indices are integrated measurements and do not take into account wavelength-dependent features within the bandpass. Therefore, skylines will severely complicate their measurement because affected wavelengths are not down-weighted. Furthermore, skylines result in non-Gaussian and correlated noise properties, and so error bars on Lick indices are usually underestimated. Consequently, Lick indices are much more prone to systematic errors. The discrepancies between individual Lick indices and the derived stellar abundance pattern based on all Lick indices for the two lower-redshift measurements further illustrate this point. By modelling the full spectrum, we use many more

features and can better deal with the larger uncertainties in regions affected by skylines.

**Code availability.** The data reduction package used to process the raw MOSFIRE data will be made public in the coming year at <http://astro.berkeley.edu/~mariska>. To derive the stellar mass, we used the flexible SPS models which are available at <https://github.com/cconroy20/fsp> and the SPS fitting code `FAST`<sup>40</sup>, which is publicly available at <http://astro.berkeley.edu/~mariska/fast/>. The spectral fitting code `alf`<sup>4,14,15</sup> that was used to derive the abundance pattern is not publicly available, but the underlying model components are available for download from <http://scholar.harvard.edu/cconroy/sps-models>.

**Data availability.** The one-dimensional original and binned spectrum shown in Figure 1 and corresponding  $1\sigma$  uncertainties, as well as the best-fitting model spectrum are available as Source Data. The binned spectrum is constructed by first masking wavelengths affected by skylines and poor atmospheric transmission, and then taking the median of the flux of ten non-masked consecutive pixels. The photometric data points shown in Figure 1 are made available by the 3D-HST collaboration (catalog version v4.1) at <http://3dhst.research.yale.edu/Data.php>. The abundance pattern for COSMOS-11494 for both the two-component and single-age model, as shown in Figure 2, is also available as Source Data.

31. Conroy, C., Gunn, J. E. & White, M. The Propagation of Uncertainties in Stellar Population Synthesis Modeling. I. The Relevance of Uncertain Aspects of Stellar Evolution and the Initial Mass Function to the Derived Physical Properties of Galaxies. *Astrophys. J.* **699**, 486–506 (2009).
32. Conroy, C. & Gunn, J. E. The Propagation of Uncertainties in Stellar Population Synthesis Modeling. III. Model Calibration, Comparison, and Evaluation. *Astrophys. J.* **712**, 833–857 (2010).
33. Kriek, M. & Conroy, C. The Dust Attenuation Law in Distant Galaxies: Evidence for Variation with Spectral Type. *Astrophys. J. Let.* **775**, L16 (2013).
34. Chabrier, G. Galactic Stellar and Substellar Initial Mass Function. *Publ. Astron. Soc. Pac.* **115**, 763–795 (2003).
35. Bruzual, G. & Charlot, S. Stellar population synthesis at the resolution of 2003. *Mon. Not. R. Astron. Soc.* **344**, 1000–1028 (2003).
36. Maraston, C. Evolutionary population synthesis: models, analysis of the ingredients and application to high- $z$  galaxies. *Mon. Not. R. Astron. Soc.* **362**, 799–825 (2005).
37. Cardelli, J. A., Clayton, G. C. & Mathis, J. S. The relationship between infrared, optical, and ultraviolet extinction. *Astrophys. J.* **345**, 245–256 (1989).
38. Calzetti, D. *et al.* The Dust Content and Opacity of Actively Star-forming Galaxies. *Astrophys. J.* **533**, 682–695 (2000).
39. Foreman-Mackey, D., Hogg, D. W., Lang, D. & Goodman, J. emcee: The MCMC Hammer. *Publ. Astron. Soc. Pac.* **125**, 306–312 (2013).
40. Kriek, M. *et al.* An Ultra-Deep Near-Infrared Spectrum of a Compact Quiescent Galaxy at  $z = 2.2$ . *Astrophys. J.* **700**, 221–231 (2009).